International Journal of Engineering Science 155 (2020) 103362

Contents lists available at ScienceDirect

International Journal of Engineering Science

journal homepage: www.elsevier.com/locate/ijengsci

Effect of saturation on the elastic properties and anisotropy of cortical bone

Jiuguang Zhou[a], Zhiwen Cui[b], Igor Sevostianov[c,*]

[a] School of Medical Science, Beihua University, Jilin 132001, China
[b] College of Physics, Jilin University, Changchun 130012, China
[c] Department of Mechanical and Aerospace Engineering, New Mexico State University, Las Cruces, NM 88003, USA

ARTICLE INFO

Article history:
Received 13 July 2020
Accepted 27 July 2020
Available online 13 August 2020

Keywords:
Cortical bone
Saturation
Anisotropy
Replacement relations

ABSTRACT

This paper focuses on the modeling of the effect of saturation on the overall elastic properties of cortical bone. We first use micromechanical model of Salguero, Saadat & Sevostianov (2014) to model anisotropic effective elastic stiffness of drained cortical bone and then apply replacement relations (see review of Sevostianov, 2020) to evaluate effect of the saturation. The model is verified by comparison with the experimental data of Granke et al. (2011). It is shown that accounting for the saturation makes the model consistent with the experiment data. We also compared the extents of anisotropy of the saturated and drained bones and show that presence of the biological fluid in pores reduces the overall anisotropy.

1. Introduction

In this paper we evaluate effect of the presence of biological liquid in bone tissue on the overall elastic properties. For this goal we combine micromechanical model for dry bone developed by Sevostianov & Kachanov (2000) and Salgueroet al., (2014) and replacement relations that link elastic properties of dry and saturated porous materials (Sevostianov & Kachanov, 2008).

Cortical bone is a heterogeneous material with hierarchical microstructure which is anisotropic at the macroscale. Most of the experimental works report orthotropic elastic properties of cortical bone (Ashman, Cowin, Van Buskirk & Rice, 1984; Bernard, Grimal & Laugier, 2013; Katz et al., 1984; Pithioux, Lasaygues & Chabrand, 2002; Rho, 1996; Van Buskirk, Cowin & Ward, 1981) which can be approximated as transversely isotropic with good accuracy (Berteau et al., 2014; Granke et al., 2011; Lang, 1969, 1970; Yoon & Katz, 1976).

Several models have been proposed in literature to evaluate mechanical properties of dry cortical bone. Stech (1967) proposed to adopt the approach used for long fiber reinforced composites and modeled cortical bone as a set of parallel cylindrical pores surrounded by layered bone tissue without any pores within the lamellae. Katz (1981) considered the effect of hierarchical structure of cortical bone on the effective elastic constants and accounted for both - the porous space modeled as a set of parallel Haversian canals and the microstructure of the dense mineralized tissue. Sevostianov & Kachanov (2000) proposed more sophisticated model based on the description of microstructure given by Martin & Burr (1989) and Currey (1984) (see also later book of Currey, 2002) that includes Haversian canals, osteocyte lacunae, Volk-

* Corresponding author.
E-mail address: igor@nmsu.edu (I. Sevostianov).

https://doi.org/10.1016/j.ijengsci.2020.103362
0020-7225/

man's canals and canaliculi was taken into account. They used compliance contribution tensors (see book of Kachanov & Sevostianov, 2018) for pores of different shapes to estimate the overall elastic constants of osteonal cortical bone in a micromechanical model approach. However, the properties of the bone dense tissue were assumed to be isotropic. Dong & Guo (2006) modeled cortical bone as a set of parallel circular Haversian canals embedded in a transversely-isotropic matrix. Martinez-Reina, Dominguez & Garcia-Aznar (2011) extended this model to include system of canaliculi on the second level. The most important aspect of this model is its ability to vary the mineral content of bone. Salguero et al. (2014) and Gao & Sevostianov (2016) extended the model of Sevostianov & Kachanov (2000) to the case of anisotropic dense tissue and considered the full set of pores existing in the cortical bone and accounted for their shapes. Modeling of the dense bone tissue as a combination of collagen fibers and crystals of hydroxyapatite has been considered in papers of (Hellmich & Ulm, 2002; Hellmich, Ulm & Dormieux, 2004; Nikolov & Raabe, 2008; Parnell, Vu, Grimal & Naili, 2012).

For the wet bone, bulk biological fluid fills the porous space (Turov et al., 2006). Fluid produces substantial impact on the mechanical properties and electrical conductivity (Casas & Sevostianov, 2013). A clear understanding of the role of saturation is yet to study. The most widely used approach to quantify the influence of pore fluids is replacement (or substitution theory first proposed by Gassmann (1951) (see (Sevostianov, 2020) for the comprehensive literature review). Cowin (1999) has applied isotropic poroelasticity model (Biot, 1941) to wet bone tissue. Isotropic poroelastic model, however, cannot explain the variability of measured wave velocities (Cardoso, Teboul, Sedel, Oddou & Meunier, 2003). Yoon & Cowin (2008a) modeled the modulus of elasticity for a single osteonal lamellae. They viewed the hydroxyapatite and collagen in the bone matrix as anisotropic poroelastic material. Yoon & Cowin (2008b) further developed the theory and evaluated the anisotropic poroelastic constants of a single osteon at the vascular porosity and lacunae-canaliculi porosity level from two perspectives: drained and saturated. This model allows one to distinguish between deformation-driven fluid movements (Cowin, 1999; Cowin & Sadegh, 1991) and the effect of liquid bound within closed pores (Hellmich, Celundova & Ulm, 2009). Martinez-Reina et al. (2011) accounted for the effects of water within the pores and compared the model of Yoon & Cowin (2008b) with experimental measurements of Tommasini, Nasser, Hu & Jepsen (2008). Faingold et al. (2014) studied the effect of saturation on the mechanical properties and structure of osteonal lamellar bone on three length scales, from the mineralized fibril level up to the osteonal level, using atomic force microscopy, nanoindentation and microindentation. They also observed that the anisotropy ratio, defined as the ratio of Young's moduli in directions parallel and perpendicular to the bone axis is lower under wet conditions than under drained ones. In contrast, Guidoni, Swain & Jäger (2010) reported no change and other authors (Seto, Gupta, Zaslansky, Wagner & Fratzl, 2008; Spiesz, Roschger & Zysset, 2012; Wolfram, Wilke & Zysset, 2010) observed an increase of this ratio with saturation. It is still an open question, whether the anisotropy ratios of dry and wet bones are the same.

In the present work, we use replacement relations to relate overall properties of drained and fully saturated cortical bone and estimate effect of the saturation on the elastic stiffness and anisotropy. We evaluate extent of anisotropy using three Thomsen's parameters (Thomsen, 1986) widely used in geophysics to describe transversely isotropic materials.

2. Elastic properties of cortical bone

2.1. Modeling of the microstructure

We model the cortical bone, following Sevostianov & Kachanov (2000) and Salguero et al. (2014) as a porous material comprised of three main systems of pores: Haversian canals, osteocyte lacunae, osteocyte canaliculi and Volkman's canals. Such a description is in accordance with the data of Currey (2002) and Fung (1993), Martin & Burr (1989). Haversian canals are modeled as a system of parallel vertical cylindrical pores in which their axes of geometrical symmetry coincide with the axes of the material symmetry of the hydroxyapatite-collagen matrix. The osteocyte lacunae, are represented by oblate spheroidal cavities randomly oriented in a plane of transverse-isotropy (planes normal to Haversian canals). Canaliculi and Volkman's canals are treated together as a set of thin horizontal cylindrical pores, with the axis of rotation perpendicular to the axis of transverse-isotropy (i.e. they are laying in planes of transvers-isotropy and are randomly oriented in these planes.

Haversian and Volkmann's canals typically constitute up to 16% of the total volume of cortical bone (Bousson et al., 2004; Kingsmill, Gray, Moles & Boyde, 2007; Thomas, Feik & Clement, 2005). The overall porosity produced by osteocyte lacunae and canaliculi in cortical bone has been reported in a range of values: 2–3.3% (Hesse et al., 2014a; 2014b; 2015; Schneider et al., 2007); 4.5% (Benalla, Palacio-Mancheno, Fritton, Cardoso & Cowin, 2014); 9–16.4% (Lin & Xu, 2011); 13.5%, 17.6%, 19% and 23% (Ashique et al., 2017; Ciani, Doty & Fritton, 2009; Kameo, Adachi, Sato & Hojo, 2010; Sharma et al., 2012). In our analysis, we first use the data of Hesse et al. (2015) for comparison with the experimental data of Granke et al. (2011). After that, we consider a wide range of porosities and examine the influence of porosity on the effective elastic moduli and anisotropy ratio.

2.2. Elastic properties of dry bone

For drained bone, we treat the pores as empty ones embedded in the dense tissue that represents a combination of collagen fibers–protein and hydroxyapatite crystals–mineral (Katz, 1980). Mineralized tissue possesses transversally isotropic mechanical properties (Currey & Zioupos, 2001). In other words, we evaluate each type of pore individually, then we sum

their contributions. The individual pore contributions for the effective elasticity are characterized by compliance contribution tensor.

Compliance contribution tensors have been first introduced in the context of ellipsoidal pores and cracks by Horii & Nemat-Nasser (1983). For the general case of elastic inhomogeneities, compliance and stiffness contribution tensors were introduced and calculated (for ellipsoidal shapes) by Sevostianov & Kachanov (1999). Sevostianov, Yilmaz, Kushch & Levin (2005) calculated components of this tensor for a spheroidal inhomogeneity embedded in a TI material. In the context of the effective elastic stiffness, the average, over representative volume V strain can be expressed as a sum:

$$\varepsilon_{ij} = S^0_{ijkl}\sigma^0_{kl} + \Delta\varepsilon_{ij} = S^0_{ijkl}\sigma^0_{kl} + \frac{V_1}{V}H_{ijkl}\sigma^0_{kl}, \tag{2.1}$$

where $S^0_{ijkl}$is the stiffness tensor of the matrix, H_{ijkl} is stiffness contribution tensor of the inhomogeneity, V_1 is the volume of the inhomogeneity, and σ^0_{kl} is the "remotely applied" stress (tractions on ∂V have the form $t_i|_{\partial V} = \sigma^0_{ij}n_j$, where σ^0_{ij} is a constant tensor and n_j is the outward unit vector normal to ∂V). For an ellipsoidal inhomogeneity, its stiffness contribution tensor is expressed in terms of Hill tensor P_{ijkl} (Hill, 1963; Walpole, 1966) as

$$H = \left[\left(S^1 - S^0\right)^{-1} + C^0 : \left(\boldsymbol{J} - \boldsymbol{P} : C^0\right)\right]^{-1} \tag{2.2}$$

Hill's tensor P_{mnrs} is related to the second gradient of the Green's tensor $G_{ij}(\boldsymbol{x} - \boldsymbol{x}')$ as

$$P_{mpij}(\boldsymbol{x}) \equiv \frac{\partial}{\partial x_{(p}} \int\limits_{V_1} \frac{\partial G_{m)(j}(\boldsymbol{x} - \boldsymbol{x}')}{\partial x'_{i)}} d\boldsymbol{x}', \tag{2.3}$$

where parentheses at subscripts denote symmetrization with respect to $m \leftrightarrow p$ and $i \leftrightarrow j$, so that tensor P_{mpij} has the same symmetry as the tensor of elastic constants. The expressions for the components of this tensor for a spheroidal inhomogeneity in a transversely-isotropic material were derived by Sevostianov et al. (2005). Components of this tensor for four types of pores forming microstructure of cortical bone are given in the Appendix.

In the case of multiple inhomogeneities, if the interaction between them is ignored, the extra compliance produced by the inhomogeneities is given by $\sum\limits_m \boldsymbol{H}^{(m)}$. If concentration of the inhomogeneities is higher than 0.15, the interaction cannot be neglected (Sevostianov & Sabina, 2007). In this case one of the approximate homogenization techniques has to be used. The most widely used schemes – effective media approaches (self-consistent and differential) or effective field schemes (Mori-Tanaka-Benveniste and Maxwell schemes) have their own bounds of applicability. The detailed analysis is given in the book of Kachanov & Sevostianov (2018). According to this analysis, the most appropriate homogenization method for anisotropic multiphase materials is Maxwell scheme in the interpretation of Sevostianov & Giraud (2013), who reformulated the Maxwell method, using the concept of property contribution tensors, as follows.

Let us cut a representative element (RVE) of volume V_Ω from a composite and place it into the matrix material. Effect produced by this element is described either by the sum of compliance contribution tensors of the inhomogeneities $\frac{1}{V}\sum\limits_i V_i\mathbf{H}_i$ or by the compliance contribution tensor $\boldsymbol{H}_{eff}$ of the entire RVE considered as an individual inhomogeneity with homogenized unknown properties. Equating these two quantities we have the general equation for the Maxwell scheme:

$$\frac{V_\Omega}{V}\boldsymbol{H}_{\boldsymbol{eff}} = \frac{1}{V}\sum_i V_i\boldsymbol{H}_{\boldsymbol{i}}. \tag{2.4}$$

The right hand side of the equation is known, however, the left hand side reflects combined effect (1) of overall properties of the RVE Ω and (2) of its shape. The main challenge in solving Eq. (2.4) is the separation of these effects that can be done analytically only in the case of the ellipsoidal shape of Ω, when according to Eq. (2.2)

$$\boldsymbol{S}^{eff} = \boldsymbol{S}^0 + \left\{\left[\frac{1}{V_\Omega}\sum_i V_i\boldsymbol{H}^{(i)}\right]^{-1} - \boldsymbol{Q}_\Omega\right\}^{-1}, \tag{2.5}$$

where

$$Q_\Omega = C^0 : \left(\boldsymbol{J} - \boldsymbol{P}_\Omega : C^0\right) \tag{2.6}$$

is second Hill's tensor of the domain Ω. Sevostianov (2014) proposed a method of evaluation of the shape of Ω that was numerically validated by Kushch & Sevostianov (2016). For a prolate spheroid in a transversely isotropic material, in particular, the aspect ratio of Ω is given by the ratio of the sums of the components of Hill's tensors for individual inhomogeneities: $\frac{\sum_i V_i P^{(i)}_{1111}}{\sum_i V_i P^{(i)}_{3333}}$.

2.3. Evaluation of the properties of saturated bone using replacement relations

Note that Hill's tensors$\boldsymbol{P}$ and $\boldsymbol{Q}$ depend only on the inhomogeneity shape (and elastic properties of the surrounding material), but *not on its elastic constants*. Thus, these equations written for two inhomogeneities "A" and "B" having the

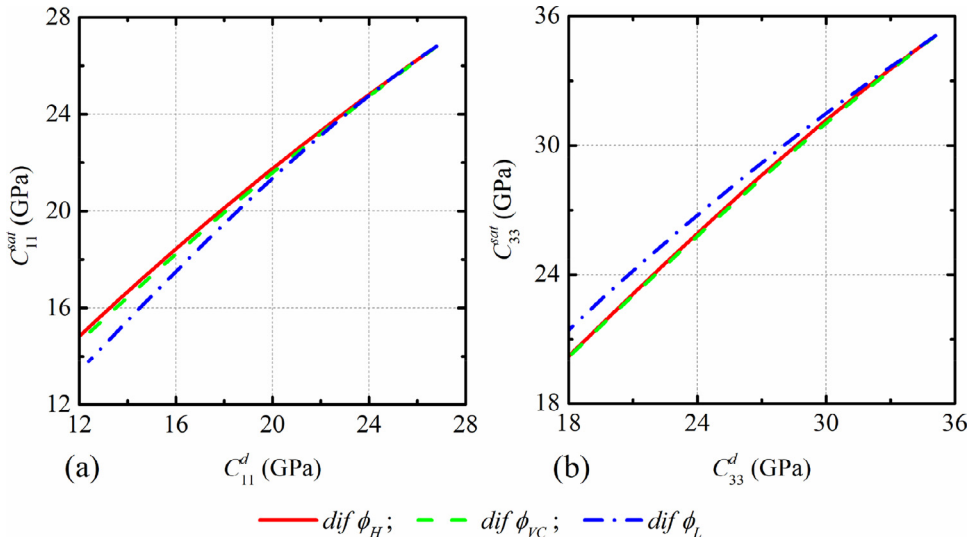

Fig. 1. The predicted saturated longitudinal mesoscopic elastic moduli of the cortical bone as a function of dry ones of the cortical bone assuming that only one partial porosity exists. The partial porosity either produced by Haversian canals, produced by Volkman's canals and canaliculi, or produced by osteocyte lacunae.

Table 1
The transversely isotropic elastic constants of fresh human femoral bone matrix calculated based on ultrasound testing done by Granke et al. (2011).

C_{11}^m (GPa)	C_{33}^m (GPa)	C_{13}^m (GPa)	C_{44}^m (GPa)	C_{66}^m (GPa)
26.8	35.1	15.3	7.3	5.8

same shape but different elastic constants (and placed in the same matrix) will contain the same $\boldsymbol{Q}$ and $\boldsymbol{P}$. Excluding $\boldsymbol{P}$ and $\boldsymbol{Q}$ from them yields the following replacement relation (Sevostianov & Kachanov, 2007):

$$\boldsymbol{H}_A^{-1} - \boldsymbol{H}_B^{-1} = (\boldsymbol{S}_A - \boldsymbol{S}_0)^{-1} - (\boldsymbol{S}_B - \boldsymbol{S}_0)^{-1} \tag{2.7}$$

In particular, if material "B" is a pore, the above relation takes the form:

$$\boldsymbol{H}_A^{-1} - \boldsymbol{H}_{pore}^{-1} = (\boldsymbol{S}_A - \boldsymbol{S}_0)^{-1} \tag{2.8}$$

Using these relations allows one to express effective elastic properties of a saturated material in terms of dry material. In particular, Maxwell scheme yields the following relations for the effective compliance tensors of dry porous material and material with filled pores

$$\boldsymbol{S}_{dry} = \boldsymbol{S}_0 + \phi \boldsymbol{H}_{pore} : [J - \phi \boldsymbol{Q}_\Omega : \boldsymbol{H}_{pore}]^{-1} \tag{2.9}$$

$$\boldsymbol{S}_{eff} = \boldsymbol{S}_0 + \phi \boldsymbol{H}_A : [J - \phi \boldsymbol{Q}_\Omega : \boldsymbol{H}_A]^{-1} \tag{2.10}$$

Replacement relation (2.8) yields then:

$$\boldsymbol{S}_{eff} = \boldsymbol{S}_0 + \phi \left[(\boldsymbol{S}_A - \boldsymbol{S}_0)^{-1} + \phi (\boldsymbol{S}_{dry} - \boldsymbol{S}_0)^{-1} \right]^{-1} \tag{2.11}$$

Fig. 1. illustrates the connection between components of the elastic stiffness tensors of dry and saturated porous materials when entire porosity is associated with one type of pores only (either ϕ_H, ϕ_{VC}, or ϕ_L) and bulk modulus of the liquid is K_f=2.25 GPa. The overall elastic stiffness of saturated material is higher than those of the dry material. The ratio C_{11}^{sat}/C_{11}^{d} is mainly affected by porosity produced by Haversian canals; the ratio C_{33}^{sat}/C_{33}^{d} is mainly affected by the porosity due to lacunae. Note, that, as shown by Chen, Sevostianov, Giraud & Grgic (2017), relation (2.11) completely coincides with the replacement relations used in geophysics (Brown & Korringa, 1975; Ciz & Shapiro, 2007; Gassmann, 1951).

3. Results and discussion

We now compare the results of the modeling with experimental data of Granke et al. (2011). Elastic stiffnesses of the bone matrix are given in Table 1. These values have been determined by Granke et al. (2011) from the wave velocities measured by pulse transmission method. The porosity was measured by Synchrotron micro CT.

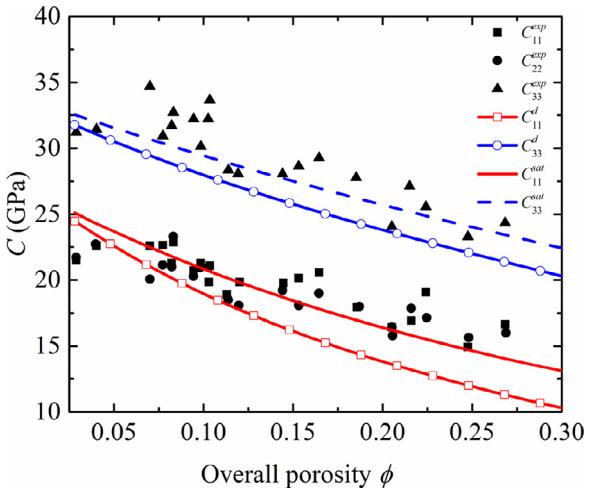

Fig. 2. Comparison of the predicted saturated and dry longitudinal mesoscopic elastic moduli of the cortical bone with experimental data of Granke et al. (2011).

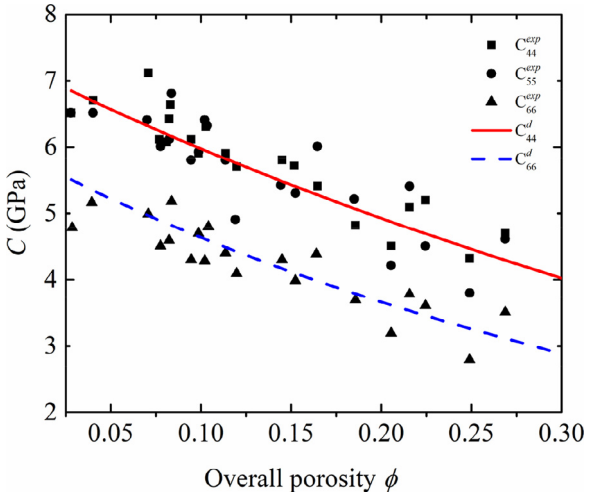

Fig. 3. Comparison of the predicted saturated and dry shear mesoscopic elastic moduli of the cortical bone with experimental data of Granke et al. (2011).

The accuracy of the prediction is evaluated using The Root Mean Square Error (*RMSE*) values:

$$RMSE = \sqrt{\frac{1}{21}\sum_{k=1}^{21}\sum_{i=1}^{6}\left(\frac{C_{ii;k}^{j} - C_{ii;k}^{EXP}}{C_{ii;k}}\right)} \times 100\%\ j = \text{dry or saturated} \tag{3.1}$$

where $C_{ii;k}^{j}$ are predicted elastic coefficients of dry or saturated bone and $C_{ii;k}^{EXP}$ their experimentally measured counterparts.

Fig. 2 illustrates comparison of the predictions of our model for normal stiffnesses with the experimental data of Granke et al. (2011) under assumption that porosity due to the osteocyte lacunae is 2.8% and aspect ratio of the lacunae is 0.3. The *RMSE* values are 0.0817 for C_{11}^{d}, 0.0450 for C_{11}^{sat}, 0.0519 for C_{22}^{d}, 0.0162 for C_{22}^{sat}, 0.0353 for C_{33}^{d}, and 0.0164 for C_{33}^{sat}. Generally, the normal effective stiffnesses of saturated bone are in better agreement with the experimental data than corresponding stiffnesses of the dry bone. Fig. 3 shows comparison with the experimental data for shear stiffnesses of the dry bone (the experimental data for saturated bone are not available). The RMSE values are 0.030 for C_{44}^{d}, 0.0265 for C_{55}^{d}, and 0.0201 for C_{66}^{d}.

Fig. 4 illustrates the extent of anisotropy measured in terms of Thomsen's parameters $\varepsilon = \frac{C_{11}-C_{33}}{2C_{33}}$ and $\gamma = \frac{C_{66}-C_{44}}{2C_{44}}$ (Thomsen, 1986) for dry and saturated cortical bone. The anisotropy ratio is found to be lower in saturated model compared to the dry ones. The result is in good agreement with the previous study (Faingold et al., 2014). The difference in the extent of anisotropy between the dry and saturated bone becomes more noticeable as the overall porosity increases.

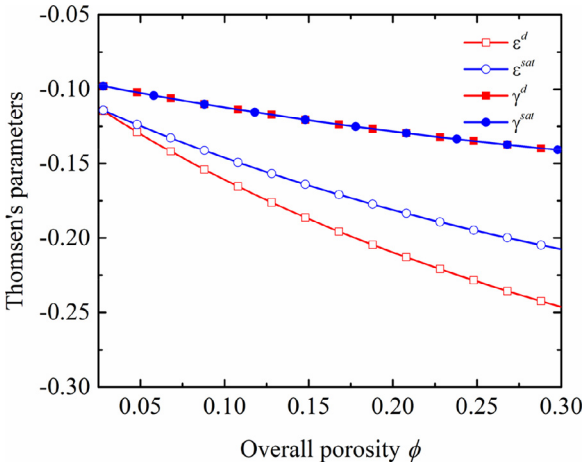

Fig. 4. omparison of the predicted mesoscopic Thomsen's parameters of the saturated and dry cortical bone, as overall porosity increases.

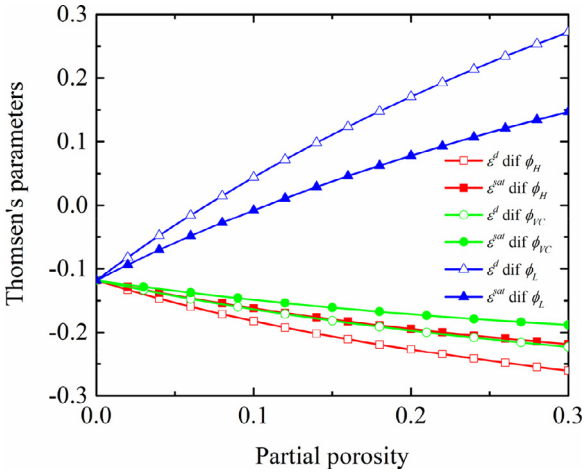

Fig. 5. The effect of the variation of the partial porosities on mesoscopic anisotropic Thomsen's parameters of dry bone (ε^d) and that of saturated bone (ε^{sat}).

Fig. 5 illustrates effect of variation of partial porosities on the Thomsen's parameter ε for dry and saturated specimens. We can observe that, as partial porosities produced by Haversian canals and canaliculi increases, both ε^d and ε^{sat} increase and ε^d is always larger than ε^{sat}. However, as lacunae porosity increase, both ε^d and ε^{sat} decrease, and ε^d is always lower than ε^{sat}. This confirms that Thomsen's parameter ε is more sensitive to changes in porosity under dry condition.

Carter, Thomas, Clement & Cooper (2013a) reported that lacunae were more flattened in the anterior and posterior regions than in the medial and lateral regions. They also found that cortical bone, in the age group under 50 years old, is characterized by flatter and less equant lacunae than those in the older group, which are more equal in dimensions (Carter et al. (2013a). Elongation does not appear affected in the older group. Therefore, we investigated the effect of the Lacunae shape on the ratio of ε^{sat} to ε^d.

Fig. 6 illustrates the effect of the aspect ratio on the saturated and dry normal effective elastic stiffnesses of the cortical bone and the ratio of the saturated elastic modulus to dry one. The aspect ratio increases from 0.1 to 10. The lacunae porosity is set to be 0.1. From the Fig. 6(a), we can observe that the curves of the saturated and the dry normal elastic moduli of the cortical bone C_{11}^{sat} and C_{11}^{d} will rise before it declines. But the curves of C_{33}^{sat} and C_{33}^{d} are monotonously ascending as aspect ratio increases. The ratio of the saturated elastic modulus to dry one C_{11}^{sat}/C_{11}^{d} is not monotonous yet, as seen from Fig. 6(b).

Fig. 7 shows the effect of the lacunae shape on Thomsen's parameters ε^d and ε^{sat}. The aspect ratio increases from 0.1 to 10. Lacunae porosity is set to 0.1. Both, ε^d and ε^{sat}, monotonously decrease as aspect ratio increases. It also can be observed that ε^{sat} is smaller than ε^d when aspect ratio is less than 1.

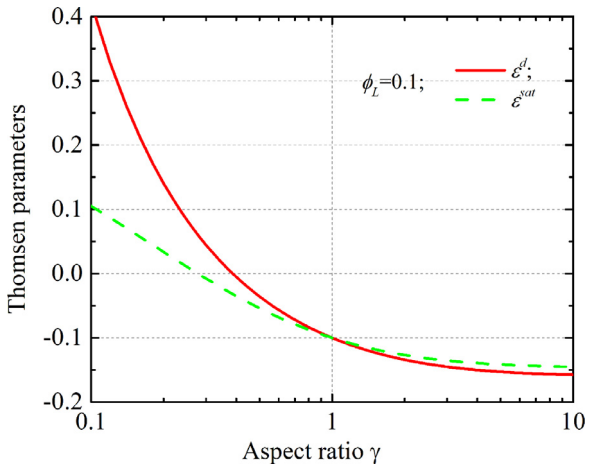

Fig. 6. The effect of the aspect ratio of lacunae pore on the saturated and dry longitudinal mesoscopic elastic moduli of the cortical bone and on the ratio of the saturated longitudinal mesoscopic elastic moduli to dry ones. (a) C_{11}^d, C_{11}^{sat}, C_{33}^d, and C_{33}^{sat}; (b) C_{11}^{sat}/C_{11}^d and C_{33}^{sat}/C_{33}^d. Lacunae porosity is set to 0.1.

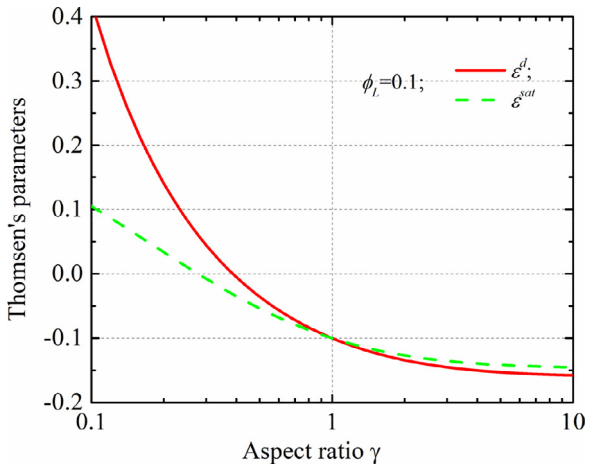

Fig. 7. The effect of the aspect ratio of lacunae pore on Thomsen's parameters ε^d and ε^{sat}. Lacunae porosity is set to 0.1.

4. Concluding remarks

This paper focuses on the effect of saturation on the elastic moduli and anisotropy ratio of cortical bone. We used Maxwell homogenization scheme to express elastic stiffnesses of fluid saturated bone in terms of the stiffnesses of dry bone, solid skeleton, and properties of the liquid. This model accounts for the effect of pore arrangement and shape. The effect of fluid flow in different pores on the moduli of saturated bone is out of scope of the present study and constitutes the next step.

It is observed that the stiffnesses of the saturated bone are higher than the ones of dry bone in contrast with the statement of Faingold et al. (2014). Note, however, that we did not account for possible changes in the properties of the bone solid phase associated with the saturation process. We compared the effect of the variation of the partial porosities on effective elastic moduli of bone under dry and saturated condition and verified the model against the experimental data of Granke et al. (2011). All the saturated normal elastic stiffnesses of the saturated bone fit better with experimental date than those of dry bone. The anisotropy ratio, as measured by Thomsen's parameters, is found to be lower in saturated bone than in the dry ones. We also illustrated effect of variation of partial porosities on Thomsen's parameters. When aspect ratio of lacunae is 0.3, extent of anisotropy decreases as lacunae porosity increases. In the context of the effect of the lacunae shape on the Thomsen's parameter ε, ε^{sat} is smaller than ε^d when the aspect ratio of the lacunae is less than 1.

Declaration of Competing Interest

The authors have no conflict of interest.

Acknowledgments

J.Z. acknowledges financial support of China Scholarship Council (# 201802325004) that allowed him to do research at NMSU, Z.C. acknowledges financial support from Natural Science Foundation of Jilin Province of China (Grant # 20180101282JC); I.S. acknowledges financial support from NSF grant #2011220.

Appendix A. Components of the compliance contribution tensor for different pores

Tables A1 and A2.

Appendix B. Compliance contribution tensor of a spheroidal pore in a transversely-isotropic material

The expressions for the components of the compliance contribution tensor for spheroidal inhomogeneity in a transversely-isotropic material were calculated by Sevostianov et al. (2005).

We consider a spheroidal pore (or inhomogeneity that is much softer than the surrounding material) with semi-axes $a_1 = a_2 \equiv a$ and a_3, and aspect ratio $\gamma = \frac{a_3}{a}$. The x_3 axis of the spheroid ($\boldsymbol{m}$ being a unit vector along it) coincides with the axis of transverse isotropy of the matrix. Compliance contribution tensor can be calculated as tensor inverse to

$$H_{ijkl} = \left[C^0_{ijmn}\left(J_{mnkl} - P_{mnrs}C^0_{rskl}\right)\right]^{-1} \tag{A.1}$$

where Hill's tensor P_{mnrs} is calculated as

$$P_{mpij}(\boldsymbol{x}) \equiv \frac{\partial}{\partial x_{(p}} \int_{\Omega} \frac{\partial G_{m)(j}(\boldsymbol{x}-\boldsymbol{x}')}{\partial x'_{i)}} d\boldsymbol{x}'$$

We write tensor P_{ijkl} in the form

$$P_{ijkl} = p_1 T^1_{ijkl} + p_2 T^2_{ijkl} + p_3 T^3_{ijkl} + p_4 T^4_{ijkl} + p_5 T^5_{ijkl} + p_6 T^6_{ijkl} \tag{A.2}$$

where basic tensors T^m_{ijkl} are given by (see Kunin (1983), Walpole (1984), Kanaun and Levin (2008)):

$$\begin{aligned} T^{(1)}_{ijkl} &= \theta_{ij}\theta_{kl}, \quad T^{(2)}_{ijkl} = \left(\theta_{ik}\theta_{lj} + \theta_{il}\theta_{kj} - \theta_{ij}\theta_{kl}\right)/2, \quad T^{(3)}_{ijkl} = \theta_{ij}m_k m_l, \\ T^{(4)}_{ijkl} &= m_i m_j \theta_{kl}, \quad T^{(5)}_{ijkl} = \left(\theta_{ik}m_l m_j + \theta_{il}m_k m_j + \theta_{jk}m_l m_i + \theta_{jl}m_k m_i\right)/4, \\ T^{(6)}_{ijkl} &= m_i m_j m_k m_l \end{aligned} \tag{A.3}$$

with $\theta_{ij} = \delta_{ij} - m_i m_j$ and m is a unit vector along the axis of transverse symmetry.

Table A1
Components of the compliance contribution tensor (GPa^{-1}) for three main microstructural elements of cortical bone.

	Single cylinder normal to the plane of isotropy		
(Haversian canal)	Single oblate spheroid (lacuna)	Single cylinder laying in the plane of isotropy (Volkman's canal & canaliculus	
H_{1111}	0.1706	0.0755	0.1480
H_{3333}	0.0417	0.2488	0.0536
H_{1122}	−0.0495	−0.0212	−0.0408
H_{1133}	−0.0152	−0.0296	−0.0185
H_{1212}	0.1100	0.0484	0.0944
H_{1313}	0.0685	0.1019	0.0720

Table A2
Components of ΣH_{ijkl} (GPa^{-1}) for three systems of pores in cortical bone (ϕ_H is partial volume fraction of Haversian canals, ϕ_{VC} is volume fraction of Volkman's canals and canaliculi, and ϕ_L is partial volume fraction of osteocyte lacunae).

	Haversian canals	Osteocyte lacunae	Volkman's canals & canaliculi
ΣH_{1111}	0.1706 ϕ_1	0.0755 ϕ_3	0.1480 ϕ_2
ΣH_{3333}	0.0417 ϕ_1	0.2488 ϕ_3	0.0536 ϕ_2
ΣH_{1122}	−0.0495 ϕ_1	−0.0212 ϕ_3	−0.0408 ϕ_2
ΣH_{1133}	−0.0152 ϕ_1	−0.0296 ϕ_3	−0.0185 ϕ_2
ΣH_{1212}	0.1100 ϕ_1	0.0484 ϕ_3	0.0944 ϕ_2
ΣH_{1313}	0.0685 ϕ_1	0.1019 ϕ_3	0.0720 ϕ_2

Coefficients p_i are as follows

$$p_1 = \frac{\pi}{2}\sum_{q=1}^{3}(b_q - A_q a_q)J_1^{(q)} \quad p_2 = \frac{\pi}{2}\sum_{q=1}^{3}(2b_q - A_q a_q)J_1^{(q)},$$
$$p_3 = p_4 = \frac{-\pi}{2}\sum_{q=1}^{3} c_q\left(J_1^{(q)} - \gamma^2 A_q J_2^{(q)}\right),$$
$$p_5 = \pi\sum_{q=1}^{3}\left[(2b_q - A_q a_q)J_2^{(q)}/\gamma^2 - c_q\left(J_1^{(q)} - A_q J_2^{(q)}/\gamma^2\right) + d_q J_1^{(q)}\right],$$
$$p_6 = 2\pi\sum_{q=1}^{3} d_q J_2^{(q)}/\gamma^2 \tag{A.4}$$

and shape factors (functions of the aspect ratio γ) are

$$J_1^{(q)} = A_q\gamma^2\int_{-1}^{1}\frac{\left(1-u^2\right)du}{\left[\gamma^2 + \left(1-\gamma^2\right)u^2\right][A_q + (1-A_q)u^2]^{3/2}} = \lambda_q^2\left[2 - A_q\frac{\lambda_q}{\gamma^2}\ln\left(\frac{\lambda_q+1}{\lambda_q-1}\right)\right]$$
$$J_2^{(q)} = A_q\int_{-1}^{1}\frac{u^2 du}{\left[1 + \left(\gamma^2-1\right)u^2\right][A_q + (1-A_q)u^2]^{3/2}} = \lambda_q^2\left[\lambda_q\ln\left(\frac{\lambda_q+1}{\lambda_q-1}\right) - 2\right] \tag{A.5}$$

where $\lambda_q = \gamma/\sqrt{\gamma^2 - A_q}$ and where coefficients a_l, b_l, c_l, d_l and A_l depend on elastic stiffnesses as follows:

$$a_l = \frac{1}{\varepsilon_l}\left[(C_{1212} - C_{1111})(C_{3333} - A_l C_{2323}) + (C_{1133} + C_{2323})^2\right]$$
$$b_l = \frac{1}{\varepsilon_l}\left[(C_{2323} - A_l C_{1111})(C_{3333} - A_l C_{2323}) + A_l(C_{1133} + C_{2323})^2\right]$$
$$c_l = \frac{1}{\varepsilon_l}(C_{1133} + C_{2323})(C_{2323} - A_l C_{1212})$$
$$d_l = \frac{1}{\varepsilon_l}(C_{2323} - A_l C_{1111})(C_{2323} - A_l C_{1212})$$
$$\varepsilon_l = 4\pi C_{1111}C_{2323}C_{1212}\prod_{j=1\ (j\neq l)}^{3}\left(A_j - A_l\right)$$
$$A_1 = C_{2323}/C_{1212} \tag{A.6}$$

and where A_2 and A_3 are roots of the quadratic equation (Elliott and Mott, 1948)

$$C_{1111}C_{2323}A^2 + \left(C_{1133}^2 + 2C_{1133}C_{2323} - C_{1111}C_{3333}\right)A + C_{2323}C_{3333} = 0 \tag{A.7}$$

In particular for strongly prolate spheroidal inhomogeneity ($\gamma \to \infty$),

$$J_1^{(q)} = 2; J_2^{(q)}/\gamma^2 \to 0 \tag{A.8}$$

and

$$\sum_{q=1}^{3} b_q = \frac{1}{2\pi C_2}; \sum_{q=1}^{3} c_q = 0; \sum_{q=1}^{3} d_q = \frac{1}{\pi C_5}; \sum_{q=1}^{3}(b_q - A_q a_q) = \frac{1}{2\pi(2C_1 + C_2)} \tag{A.9}$$

Substitution of (3.4.21) and (3.4.17) into (3.4.12) leads to the following coefficients of representation of tensor $\boldsymbol{P}$ in the standard tensor basis:

$$p_1^0 = \frac{1}{2(2C_1 + C_2)}; p_2^0 = \frac{1}{2(2C_1 + C_2)} + \frac{1}{2C_2}; p_5^0 = 2/C_5$$
$$p_3^0 = p_4^0 = p_6^0 = 0$$

In particular, if the matrix material is *isotropic*, we recover known result (Sevostianov and Kachanov, 1999)

$$P_{1111} = P_{2222} = \frac{4-3\kappa}{8\mu}, P_{1122} = P_{2211} = \frac{-\kappa}{8\mu}, P_{1212} = \frac{2-\kappa}{8\mu},$$
$$P_{1313} = P_{2323} = \frac{1}{8\mu}, P_{3333} = P_{1133} = P_{2233} = P_{3311} = P_{3322} = 0$$

Where μ is the shear modulus and κ is connected with the Poisson's ratio ν as $\kappa = \frac{1}{[2(1-\nu)]}$

For inhomogeneities not aligned with the symmetry axis of the matrix, like Volkman's canals and canaliculi, we use analytical approximation for components of tensor H_{ijkl} following approach proposed by Saadat et al. (2012). We first find the best isotropic approximation for a transversely isotropic tensor of elastic stiffness C_{ijkl} (see Fedorov, 1968) given by

$$\lambda_0 \delta_{ij}\delta_{kl} + G_0\left(\delta_{ik}\delta_{lj} + \delta_{il}\delta_{kj}\right) \tag{A.11}$$

where

$$G_0 = (3C_{ikik} - C_{iikk})/30, \lambda_0 = (2C_{iikk} - C_{ikik})/15 \tag{A.12}$$

Using this best fit isotropy, we can calculate the components of the compliance contribution tensor for a spheroidal inclusion with semi axis $a_1 = a_2 = a$, and a_3 embedded in the matrix characterized by elastic constants G_0 and λ_0. For a pore or very soft inclusion coefficients in the representation $\boldsymbol{H} = \sum_{k=1}^{6} h_k \boldsymbol{T}^{(k)}$ take the form (Sevostianov et al., 2006)

$$h_1 = \frac{\kappa(f_0 - f_1)}{2G_0(4\kappa-1)\left[2\kappa(f_0-f_1) - (4\kappa-1)f_0^2\right]};$$
$$h_2 = \frac{1}{2G_0[1-(2-\kappa)f_0 - \kappa f_1]};$$
$$h_3 = h_4 = \frac{-(2\kappa f_0 - f_0 + 2\kappa f_1)}{4G_0(4\kappa-1)\left[2\kappa(f_0-f_1) - (4\kappa-1)f_0^2\right]};$$
$$h_5 = \frac{4}{4G_0[f_0 + 4\kappa f_1]};$$
$$h_6 = \frac{4\kappa - 1 - 6\kappa f_0 + 2f_0 - 2\kappa f_1}{4G_0(4\kappa-1)\left[2\kappa(f_0-f_1) - (4\kappa-1)f_0^2\right]} \tag{A.13}$$

where

$$\kappa = \frac{\lambda_0 + G_0}{\lambda_0 + 2G_0}; f_0 = \frac{\gamma^2(1-g)}{2\left(\gamma^2-1\right)}, f_1 = \frac{\gamma^2}{4\left(\gamma^2-1\right)^2}\left[\left(2\gamma^2+1\right)g - 3\right] \tag{A.14}$$

and the shape factor g is expressed in terms of the aspect ratio $\gamma = a_3/a$ as follows

$$g(\gamma) = \begin{cases} \frac{1}{\gamma\sqrt{1-\gamma^2}} \arctan\frac{\sqrt{1-\gamma^2}}{\gamma}, & \text{oblate shape } (\gamma < 1) \\ \frac{1}{2\gamma\sqrt{\gamma^2-1}} \ln\frac{\gamma+\sqrt{\gamma^2-1}}{\gamma-\sqrt{\gamma^2-1}}, & \text{prolate shape } (\gamma > 1) \end{cases} \tag{A.15}$$

The best isotropic approximation for the elastic constants in Table 1 is provided by $G_0 = 6.940 GPa$ and $\lambda_0 = 15.407\ GPa$.

References

Ashique, A. M., Hart, L. S., Thomas, C. D. L., Clement, J. G., Pivonka, P., Carter, Y., et al. (2017). Lacunar-canalicular network in femoral cortical bone is reduced in aged women and is predominantly due to a loss of canalicular porosity. *Bone Reports, 7*, 9–16.

Ashman, R. B., Cowin, S. C., Van Buskirk, W. C., & Rice, J. C. (1984). A continuous wave technique for the measurement of the elastic properties of cortical bone. *Journal of Biomechanics, 17*(5), 349–361.

Benalla, M., Palacio-Mancheno, P. E., Fritton, S. P., Cardoso, L., & Cowin, S. C. (2014). Dynamic permeability of the lacunar-canalicular system in human cortical bone. *Biomechanics and Modeling in Mechanobiology, 13*(4), 801–812.

Bernard, S., Grimal, Q., & Laugier, P. (2013). Accurate measurement of cortical bone elasticity tensor with resonant ultrasound spectroscopy. *Journal of the Mechanical Behavior of Biomedical Materials, 18*, 12–19.

Berteau, J. P., Baron, C., Pithioux, M., Launay, F., Chabrand, P., & Lasaygues, P. (2014). In vitro ultrasonic and mechanic characterization of the modulus of elasticity of children cortical bone. *Ultrasonics, 54*(5), 1270–1276.

Biot, M. A. (1941). General theory of three-dimensional consolidation. *Journal of Applied Physics, 12*(2), 155–164.

Bousson, V., Peyrin, F., Bergot, C., Hausard, M., Sautet, A., & Laredo, J. D. (2004). Cortical bone in the human femoral neck: Three-dimensional appearance and porosity using synchrotron radiation. *Journal of Bone and Mineral Research : The Official Journal of the American Society for Bone and Mineral Research, 19*(5), 794–801.

Brown, R. J. S., & Korringa, J. (1975). On the dependence of the elastic properties of a porous rock on the compressibility of the pore fluid. *Geophysics, 40*(4), 608–616.

Cardoso, L., Teboul, F., Sedel, L., Oddou, C., & Meunier, A. (2003). In vitro acoustic waves propagation in human and bovine cancellous bone. *Journal of Bone and Mineral Research : The Official Journal of the American Society for Bone and Mineral Research, 18*(10), 1803–1812.

Carter, Y., Thomas, C. D. L., Clement, J. G., & Cooper, D. M. L. (2013a). Femoral osteocyte lacunar density, volume and morphology in women across the lifespan. *Journal of Structural Biology, 183*(3), 519–526.
Casas, R., & Sevostianov, I. (2013). Electrical resistivity of cortical bone: micromechanical modeling and experimental verification. *International Journal of Engineering Science, 62*, 106–112.
Chen, F., Sevostianov, I., Giraud, A., & Grgic, D. (2017). Accuracy of the replacement relations for materials with non-ellipsoidal inhomogeneities. *International Journal of Solids and Structures, 104-105*, 73–80.
Ciani, C., Doty, S. B., & Fritton, S. P. (2009). An effective histological staining process to visualize bone interstitial fluid space using confocal microscopy. *Bone, 44*(5), 1015–1017.
Ciz, R., & Shapiro, S. A. (2007). Generalization of Gassmann equations for porous media saturated with a solid material. *Geophysics, 72*(6), A75–A79.
Cowin, S. C. (1999). Bone poroelasticity. *Journal of Biomechanics, 32*(3), 217–238.
Cowin, S. C., & Sadegh, A. M. (1991). Non-interacting modes for stress, strain and energy in anisotropic hard tissue. *Journal of Biomechanics, 24*(9), 859–867.
Currey, J. D. (1984). *The mechanical adaptations of bones*. Princeton, New Jersey: Princeton University Press.
Currey, J. D. (2002). *Bones: Structure and mechanics*. New York: Princeton University Press.
Currey, J. D., & Zioupos, P. (2001). The effect of porous microstructure on the anisotropy of bone-like tissue. *Journal of Biomechanics, 34*(5), 707–708.
Dong, X. N., & Guo, X. E. (2006). Prediction of cortical bone elastic constants by a two-level micromechanical model using a generalized self-consistent method. *Journal of Biomechanical Engineering, 128*(3), 309–316.
Elliott, H. A., & Mott, N. F. (1948). Three-dimensional stress distributions in hexagonal aeolotropic crystals. *Mathematical Proceedings of the Cambridge Philosophical Society, 44*(4), 522–533.
Faingold, A., Cohen, S. R., Shahar, R., Weiner, S., Rapoport, L., & Wagner, H. D. (2014). The effect of hydration on mechanical anisotropy, topography and fibril organization of the osteonal lamellae. *Journal of Biomechanics, 47*(2), 367–372.
Fedorov, F. I. (1968). *Theory of elastic waves in crystals*. New York: Plenum Press.
Fung, Y. C. (1993). *Biomechanics: Mechanical properties of living tissues*. New York: Springer.
Gao, X., & Sevostianov, I. (2016). Connection between elastic and electrical properties of cortical bone. *Journal of Biomechanics, 49*(5), 765–772.
Gassmann, F. (1951). Über die Elastizität poröser Medien. *Vierteljahrschrift der Naturforschenden Gessellschaft in Zürich, 96*, 1–23.
Granke, M., Grimal, Q., Saied, A., Nauleau, P., Peyrin, F., & Laugier, P. (2011). Change in porosity is the major determinant of the variation of cortical bone elasticity at the millimeter scale in aged women. *Bone, 49*(5), 1020–1026.
Guidoni, G., Swain, M., & Jäger, I. (2010). Nanoindentation of wet and dry compact bone: Influence of environment and indenter tip geometry on the indentation modulus. *Philosophical Magazine, 90*(5), 553–565.
Hellmich, C., Celundova, D., & Ulm, F.-. J. (2009). Multiporoelasticity of hierarchically structured materials: micromechanical foundations and application to bone. *Journal of Engineering Mechanics ASCE, 135*(5), 382–394.
Hellmich, C., & Ulm, F.-. J. (2002). Micromechanical model for ultrastructural stiffness of mineralized tissues. *Journal of Engineering Mechanics -ASCE, 128*(8), 898–908.
Hellmich, C., Ulm, F. J., & Dormieux, L. (2004). Can the diverse elastic properties of trabecular and cortical bone be attributed to only a few tissue-independent phase properties and their interactions? Arguments from a multiscale approach. *Biomechanics and Modeling in Mechanobiology, 2*(4), 219–238.
Hesse, B., Langer, M., Varga, P., Pacureanu, A., Dong, P., Schrof, S., et al. (2014a). Alterations of mass density and 3D osteocyte lacunar properties in bisphosphonate-related osteonecrotic human jaw bone, a synchrotron microCT study. *Plos One, 9*(2), e88481.
Hesse, B., Mannicke, N., Pacureanu, A., Varga, P., Langer, M., Maurer, P., et al. (2014b). Accessing osteocyte lacunar geometrical properties in human jaw bone on the submicron length scale using synchrotron radiation muCT. *Journal of Microscopy, 255*(3), 158–168.
Hesse, B., Varga, P., Langer, M., Pacureanu, A., Schrof, S., Mannicke, N., et al. (2015). Canalicular network morphology is the major determinant of the spatial distribution of mass density in human bone tissue: Evidence by means of synchrotron radiation phase-contrast nano-CT. *Journal of Bone and Mineral Research: The Official Journal of the American Society for Bone and Mineral Research, 30*(2), 346–356.
Hill, R. (1963). Elastic properties of reinforced solids: Some theoretical principles. *Journal of the Mechanics and Physics of Solids, 11*(5), 357–372.
Horii, H., & Nemat-Nasser, S. (1983). Overall moduli of solids with microcracks: Load-induced anisotropy. *Journal of the Mechanics and Physics of Solids, 31*(2), 155–171.
Kachanov, M., & Sevostianov, I. (2018). Micromechanics of materials, with applications. *Solid mechanics and its applications*. Cham: Springer.
Kameo, Y., Adachi, T., Sato, N., & Hojo, M. (2010). Estimation of bone permeability considering the morphology of lacuno-canalicular porosity. *Journal of the Mechanical Behavior of Biomedical Materials, 3*(3), 240–248.
Kanaun, S.K., .& Levin, V.M. (.2008). Self-consistent methods for composites: Solid mechanics and its applications.
Katz, J. L. (1980). Anisotropy of Young's modulus of bone. *Nature, 283*, 106–107.
Katz, J. L., & Cowin, S. C. (1981). Composite material models for cortical bone. In *Mechanical properties of bone: 45* (pp. 171–184). New York: ASME.
Katz, J. L., Yoon, H. S., Lipson, S., Maharidge, R., Meunier, A., & Christel, P. (1984). The effects of remodeling on the elastic properties of bone. *Calcified Tissue International, 36*, S31–S36.
Kingsmill, V. J., Gray, C. M., Moles, D. R., & Boyde, A. (2007). Cortical vascular canals in human mandible and other bones. *Journal of Dental Research, 86*(4), 368–372.
Kunin, I.A. (.1983). Elastic media with microstructure II: Springer series in solid-state sciences.
Kushch, V. I., & Sevostianov, I. (2016). The "rigorous" Maxwell homogenization scheme in 2D elasticity: Effective stiffness tensor of composite with elliptic inhomogeneities. *Mechanics of Materials, 103*, 44–54.
Lang, S. B. (1969). Elastic coefficients of animal bone. *Science (New York, N.Y.), 165*, 287–288.
Lang, S. B. (1970). Ultrasonic method for measuring elastic coefficients of bone and results on fresh and dried bovine bones. *Ieee Transactions on Bio-Medical Engineering, 17*(2), 101–105.
Lin, Y., & Xu, S. (2011). AFM analysis of the lacunar-canalicular network in demineralized compact bone. *Journal of Microscopy, 241*(3), 291–302.
Martin, R. B., & Burr, D. B. (1989). *Structure function, and adaptation of compact bone*. New York: Raven Press.
Martinez-Reina, J., Dominguez, J., & Garcia-Aznar, J. M. (2011). Effect of porosity and mineral content on the elastic constants of cortical bone: A multiscale approach. *Biomechanics and Modeling in Mechanobiology, 10*(3), 309–322.
Nikolov, S., & Raabe, D. (2008). Hierarchical modeling of the elastic properties of bone at submicron scales: The role of extrafibrillar mineralization. *Biophysical Journal, 94*(11), 4220–4232.
Parnell, W. J., Vu, M. B., Grimal, Q., & Naili, S. (2012). Analytical methods to determine the effective mesoscopic and macroscopic elastic properties of cortical bone. *Biomechanics and Modeling in Mechanobiology, 11*(6), 883–901.
Pithioux, M., Lasaygues, P., & Chabrand, P. (2002). An alternative ultrasonic method for measuring the elastic properties of cortical bone. *Journal of Biomechanics, 35*(7), 961–968.
Rho, J. Y. (1996). An ultrasonic method for measuring the elastic properties of human tibial cortical and cancellous bone. *UltrasonicsUltrasonics, 34*(8), 777–783.
Saadat, F., Sevostianov, I., & Giraud, A. (2012). Approximate representation of a compliance contribution tensor for a cylindrical inhomogeneity normal to the axis of symmetry of a transversely isotropic material. *International Journal of Fracture, 174*(2), 237–244.
Salguero, L., Saadat, F., & Sevostianov, I. (2014). Micromechanical modeling of elastic properties of cortical bone accounting for anisotropy of dense tissue. *Journal of Biomechanics, 47*(13), 3279–3287.
Schneider, P., Stauber, M., Voide, R., Stampanoni, M., Donahue, L. R., & Muller, R. (2007). Ultrastructural properties in cortical bone vary greatly in two inbred strains of mice as assessed by synchrotron light based micro- and nano-CT. *Journal of Bone and Mineral Research : The Official Journal of the American Society for Bone and Mineral Research, 22*(10), 1557–1570.

Seto, J., Gupta, H. S., Zaslansky, P., Wagner, H. D., & Fratzl, P. (2008). Tough lessons from bone: extreme mechanical anisotropy at the mesoscale. *Advanced Functional Materials, 18*(13), 1905–1911.
Sevostianov, I. (2014). On the shape of effective inclusion in the Maxwell homogenization scheme for anisotropic elastic composites. *Mechanics of Materials, 75*, 45–59.
Sevostianov, I. (2020). Gassmann equation and replacement relations in micromechanics: A review. *International Journal of Engineering Science, 154*, 1–46. In press.
Sevostianov, I., & Giraud, A. (2013). Generalization of Maxwell homogenization scheme for elastic material containing inhomogeneities of diverse shape. *International Journal of Engineering Science, 64*, 23–36.
Sevostianov, I., & Kachanov, M. (1999). Compliance tensors of ellipsoidal inclusions. *International Journal of Fracture, 96*, L3–L7.
Sevostianov, I., & Kachanov, M. (2000). Impact of the porous microstructure on the overall elastic properties of the osteonal cortical bone. *Journal of Biomechanics, 33*(7), 881–888.
Sevostianov, I., & Kachanov, M. (2007). Relations between compliances of inhomogeneities having the same shape but different elastic constants. *International Journal of Engineering Science, 45*(10), 797–806.
Sevostianov, I., & Kachanov, M. (2008). On approximate symmetries of the elastic properties and elliptic orthotropy. *International Journal of Engineering Science, 46*(3), 211–223.
Sevostianov, I., Kováčik, J., & Simančík, F. (2006). Elastic and electric properties of closed-cell aluminum foams. *Materials Science and Engineering: A, 420*, 87–99.
Sevostianov, I., & Sabina, F. J. (2007). Cross-property connections for fiber reinforced piezoelectric materials with anisotropic constituents. *International Journal of Engineering Science, 45*(9), 719–735.
Sevostianov, I., Yilmaz, N., Kushch, V. I., & Levin, V. M. (2005). Effective elastic properties of matrix composites with transversely-isotropic phases. *International Journal of Solids and Structures, 42*(2), 455–476.
Sharma, D., Ciani, C., Marin, P. A., Levy, J. D., Doty, S. B., & Fritton, S. P. (2012). Alterations in the osteocyte lacunar-canalicular microenvironment due to estrogen deficiency. *Bone, 51*(3), 488–497.
Spiesz, E. M., Roschger, P., & Zysset, P. K. (2012). Elastic anisotropy of uniaxial mineralized collagen fibers measured using two-directional indentation. Effects of hydration state and indentation depth. *Journal of the Mechanical Behavior of Biomedical Materials, 12*, 20–28.
Stech, E. L., & Byars, E. F. (1967). A descriptive model of lamellar bone anisotropy. *Biomechanics monograph*. NewYork: AMSE.
Thomas, C. D., Feik, S. A., & Clement, J. G. (2005). Regional variation of intracortical porosity in the midshaft of the human femur: Age and sex differences. *Journal of Anatomy, 206*(2), 115–125.
Thomsen, L. (1986). Weak elastic anisotropy. *Geophysics, 51*(10), 1954–1966.
Tommasini, S. M., Nasser, P., Hu, B., & Jepsen, K. J. (2008). Biological co-adaptation of morphological and composition traits contributes to mechanical functionality and skeletal fragility. *Journal of Bone and Mineral Research : The Official Journal of the American Society for Bone and Mineral Research, 23*(2), 236–246.
Turov, V. V., Gun'ko, V. M., Zarko, V. I., Leboda, R., Jablonski, M., Gorzelak, M., et al. (2006). Weakly and strongly associated nonfreezable water bound in bones. *Colloids and Surfaces. B, Biointerfaces, 48*(2), 167–175.
Van Buskirk, W. C., Cowin, S. C., & Ward, R. N. (1981). Ultrasonic measurement of orthotropic elastic constants of bovine femoral bone. *Journal of Biomechanical Engineering, 103*(2), 67–72.
Walpole, L. J. (1966). On bounds for the overall elastic moduli of inhomogeneous systems—I. *Journal of the Mechanics and Physics of Solids, 14*(3), 151–162.
Walpole, L. J. (1984). Fourth-rank tensors of the thirty-two crystal classes: Multiplication tables. *Proceedings of the Royal Society of London. A. Mathematical and Physical Sciences, 391*, 149–179.
Wolfram, U., Wilke, H. J., & Zysset, P. K. (2010). Rehydration of vertebral trabecular bone: Influences on its anisotropy, its stiffness and the indentation work with a view to age, gender and vertebral level. *Bone, 46*(2), 348–354.
Yoon, H. S., & Katz, J. L. (1976). Ultrasonic wave propagation in human cortical bone—II. Measurements of elastic properties and microhardness. *Journal of Biomechanics, 9*(7), 459–464.
Yoon, Y. J., & Cowin, S. C. (2008a). The estimated elastic constants for a single bone osteonal lamella. *Biomechanics and Modeling in Mechanobiology, 7*, 1–11.
Yoon, Y. J., & Cowin, S. C. (2008b). An estimate of anisotropic poroelastic constants of an osteon. *Biomechanics and Modeling in Mechanobiology, 7*, 13–26.